Singularity Subtraction for Evaluation of Green's Functions for Multilayer Media

Ergün Şimşek, *Student Member, IEEE*, Qing Huo Liu, *Fellow, IEEE*, and Baojun Wei

***Abstract*—This paper presents an efficient method to evaluate the two- and three-dimensional multilayered medium Green's functions for general electric and magnetic sources. Without finding any surface poles or steepest descent path, a special subtraction procedure is applied to each term of the Sommerfeld integrands to make them rapidly decreasing functions of k_ρ. The contributions of the subtracted terms are calculated analytically. The remaining integrals are computed adaptively by using Gaussian quadratures. The accuracy of the method has been confirmed by comparison with many examples in literature, and the high efficiency has been verified.**

***Index Terms*—Green's functions, layered media.**

I. Introduction

IN ORDER to solve layered-medium problems in application areas such as geophysical prospecting and remote sensing [1]–[3], interconnect simulations, microstrip antennas and monolithic microwave integrated circuits [4]–[6], and vector and scalar Green's functions must be computed. Straightforward numerical integration methods are not efficient for these integrals because of the slowly decaying and highly oscillating behavior of the Sommerfeld integrands [7]–[11]. Extensive research has been done to accelerate this process through methods such as the fast Hankel transform (FHT) approach [12], [13], the window function approach [14], the steepest descent path (SDP) approach [2], and the discrete complex image method (DCIM) [15]–[29].

It is shown that the efficiency of the numerical integration can be improved by deforming the integration path in the complex k_ρ plane and using the Hankel functions pair instead of Bessel functions [11]. Deforming the integration path according to Cauchy's theorem avoids the singularities; it has been used in most recent methods. The usage of the Hankel functions pair helps for the faster convergence, especially when the source and field points are close to each other. In terms of the computation time, the numerical integration method is the slowest one with respect to other methods. In the SDP approach, the integration path is also deformed [2]. In addition to path deformation, leading order approximation has been used to increase the speed of integration. The difficulty related to the implementation of this method is the determination of the steepest path for the media having many layers.

Manuscript received January 31, 2005; revised June 9, 2005 and September 7, 2005. This work was supported by the National Science Foundation under Grant CCR-00-98140 and Grant IIS-0086075.

The authors are with the Department of Electrical and Computer Engineering, Duke University, Durham, NC 27708-0291 USA (e-mail: qhliu@ee.duke.edu).

Digital Object Identifier 10.1109/TMTT.2005.860304

The window function approach utilizes a window function as a convolution kernel to the time-domain Green's function [14]. Similar to the effect of low-pass filtering used in signal processing, convolution with a window function in the spatial domain accelerates the decay of integrand in the Sommerfeld integration.

The DCIM, which can be described as the approximation of the spectral-domain Green's function in terms of complex exponentials whose Hankel transform can be obtained analytically, is one of the most popular methods developed to approximate the Green's functions efficiently. It has been improved by the help of several researchers over the last two decades. In the very beginning, the primary and quasi-static field terms are subtracted from the integrand and the remaining integrand is approximated with the complex images via Sommerfeld identity. However, since the method was constructed on the Sommerfeld identity, it is not applicable to problems having source and field points in different layers because of the $k_{z,n}$ dependence in the Sommerfeld identity. Furthermore, the method was valid only for the symmetrical (i.e., diagonal) components of the dyadic Green's functions (DGFs). Hojjat *et al.* extended the method to the nonsymmetrical (i.e., off-diagonal) components by using a semi-infinite integral of Bessel functions [25]. More recently, Eselle and Ge [29] proposed a new closed-form formulation based on a class of semi-infinite integrals of Bessel functions and applied the generalized pencil of function (GPOF) method to approximate the remaining integrand with another set of complex images (having only k_ρ dependence), making the method valid for any kind of source-field point combination. Aksun has shown that, by using a multilevel DCIM, it is possible to obtain very accurate results for printed structures without subtraction of the primary and quasi-static field terms [23]. However, the lack of surface-wave extraction often results in errors in the far-field region because the surface waves behave in the manner of cylindrical waves and, thus, it is inappropriate to approximate them by spherical waves. In other words, DCIM without any extraction might work efficiently for printed-circuit structures, but cannot handle the problems such as aerospace applications where the object size is comparable to or much larger than the wavelength. Ling proposed a new method to achieve the surface-wave extraction by evaluating a contour integral recursively in the complex k_ρ plane [26]. Moreover, some researchers developed new formulations to increase the efficiency of the method for the method of moments (MOM) implementation. For example, Liu *et al.* [28] reformulated the formulation-C Green's functions for multilayered media to extract the z-dependent part when the source and observation points are in different layers.

All of these methods have some advantages and disadvantages. In this paper, a new extraction procedure is presented,

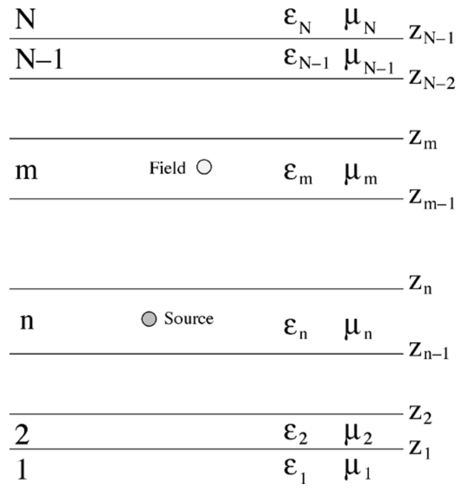

Fig. 1. N-layer medium with source and field points in layer n and layer m, respectively.

which can be incorporated in these methods to improve the efficiency. This procedure can be described as the improved version of the extraction procedure implemented in DCIM, and is valid for any kind of source-field point combination. The subtraction procedure is implemented appropriately for each individual term of the integrand and the contribution of the subtracted terms is calculated analytically. However, for the sake of robustness, instead of approximating the remaining integral with complex images, the remaining integral is calculated numerically by using Gaussian quadratures. The results of this method have been validated by comparison with many examples in literature, and the high efficiency has been verified.

II. Theory

Consider a general multilayer medium consisting of N layers separated by $N-1$ planar interfaces parallel to the xy-plane, as shown in Fig. 1. Layer i exists between z_i and z_{i-1} and is characterized by relative permittivity $\epsilon_{r,i}$ and relative permeability $\mu_{r,i}$. In a linear medium, electric and magnetic fields due to arbitrary electric and magnetic currents ($\mathbf{J}$ and $\mathbf{M}$, respectively) can be expressed as

$$\mathbf{E} = \left\langle \tilde{\tilde{\mathbf{G}}}^{EJ}; \mathbf{J} \right\rangle + \left\langle \tilde{\tilde{\mathbf{G}}}^{EM}; \mathbf{M} \right\rangle \tag{1}$$

$$\mathbf{H} = \left\langle \tilde{\tilde{\mathbf{G}}}^{HJ}; \mathbf{J} \right\rangle + \left\langle \tilde{\tilde{\mathbf{G}}}^{HM}; \mathbf{M} \right\rangle \tag{2}$$

where $\tilde{\tilde{\mathbf{G}}}^{PQ}(\mathbf{r}, \mathbf{r}')$ is the DGF relating P-type fields at $\mathbf{r}$ due to Q-type currents at $\mathbf{r}'$ [33]. Once the DGFs have been calculated for the layered medium, the electric and magnetic fields at any point can be obtained with the superposition principle. For the details of the derivation procedure of the multilayer media Green's functions, the reader may refer to [33] and [35]. Basically, by transforming the problem from the spatial to spectral domain, each layer can be represented by a uniform transmission line having the same physical properties; hence, the electric and magnetic fields can be interpreted as voltage and current, respectively, on a transmission line. By using this transmission-line analogy, Green's functions in the spectral domain, called transmission-line Green's functions (TLGFs), can be calculated easily. The spatial-domain DGF is the inverse transformation from the spectral to spatial domain and is known as a Sommerfeld integral given by

$$G_{\zeta,\eta}(\boldsymbol{\rho}, z|z') = \frac{1}{2\pi} \int_0^\infty \tilde{G}_{\zeta,\eta}(\mathbf{k}_\rho, z|z') J_\nu(k_\rho \rho) k_\rho^{\nu+1} dk_\rho \tag{3}$$

where $\nu = 0, 1$, J_ν is the νth-order Bessel function, $\rho = \sqrt{(x-x')^2 + (y-y')^2}$, $G_{\zeta,\eta}(\rho, z|z')$ is the spatial-domain Green's function relating the field at (x, y, z) in layer m due to a point source at (x', y', z') in layer n, and $\tilde{G}_{\zeta,\eta}(\mathbf{k}_\rho, z|z')$ is the spectral-domain counterpart.

III. Spatial-Domain Green's Functions

There are several types of DGFs [33]. In this paper, the traditional form of DGFs for vector potential $\mathbf{A}$ is chosen as an example and the formulation of the spectral-domain Green's functions is presented in the Appendix. The spatial-domain Green's functions are obtained by taking the Sommerfeld integral given in (3). In general, we have two typical integrals for the spatial-domain Green's functions associated with the vector and scalar potentials

$$I_1 = \int_0^\infty \xi_1(k_\rho, k_{z,m}) \frac{e^{-jk_{z,n}\alpha}}{k_{z,n}} J_0(k_\rho \rho) k_\rho dk_\rho \tag{4}$$

for symmetrical components of the Green's function, and

$$I_2 = \int_0^\infty \xi_2(k_\rho, k_{z,m}) e^{-jk_{z,n}\alpha} J_1(k_\rho \rho) dk_\rho \tag{5}$$

for nonsymmetrical components of the Green's function, where $\xi_i(k_\rho, k_{z,m})$ contains the generalized reflection coefficients and some constants depending on the type of Green's functions involved. Below we describe the singularity subtraction for different scenarios depending on where the relative locations of the source and field points.

A. Source and Field Points in the Same Layer

When the source and field points are located in the same layer ($n = m$), the Green's function can be separated into the primary and reflected field. The singularity subtraction is only needed for the reflected field, as the primary field terms are obtained directly from the expressions for a homogeneous medium. In this case, for the primary-field term, $\xi_i(k_\rho, k_{z,m})$ is constant and equal to $1/2\pi$ and, as in DCIM, the contribution of this component can be calculated analytically by using Sommerfeld identity as follows:

$$\int_0^\infty \frac{e^{-jk_{z,n}\alpha}}{k_{z,n}} J_0(k_\rho \rho) k_\rho dk_\rho = \frac{e^{-jk_n r}}{r} \tag{6}$$

where $r = \sqrt{\rho^2 + \alpha^2}$ and α is some distance.

For the reflection terms, $\xi_i(k_\rho, k_{z,m})$ is not a constant, but its asymptotic expression can be obtained by

$$\lim_{k_\rho\to\infty}\begin{cases} k_{z,i}=k_{z,j}=-jk_\rho \\ \Gamma_{i,j}=R_{i,j} \\ \xi_i(k_\rho,k_{z,m})=\tilde{\xi}_i \end{cases} \tag{7}$$

where $\tilde{\xi}_i$ is a finite constant and $\Gamma_{i,j}$ and $R_{i,j}$ are the generalized and Fresnel reflection coefficients, respectively, between layer-i and layer-j.

Using (7) in (4) yields

$$\begin{aligned} I_1 &= \int_0^\infty \left[\xi_1(k_\rho,k_{z,m})e^{-jk_{z,n}\alpha} - \tilde{\xi}_1 e^{-jk_{z,n}\alpha} + \tilde{\xi}_1 e^{-jk_{z,n}\alpha}\right] \\ &\qquad \times \frac{k_\rho}{k_{z,n}} J_0(k_\rho\rho)dk_\rho \\ &= \int_0^\infty \left[\xi_1(k_\rho,k_{z,m})e^{-jk_{z,n}\alpha} - \tilde{\xi}_1 e^{-jk_{z,n}\alpha}\right] \\ &\qquad \times \frac{k_\rho}{k_{z,n}} J_0(k_\rho\rho)dk_\rho + \frac{\tilde{\xi}_1 e^{-jk_n r}}{r} \end{aligned} \tag{8}$$

where $\tilde{\xi}_1 = \lim_{k_\rho\to\infty}\xi_1(k_\rho,k_{z,m})$. This subtraction process is valid for the symmetrical components of the DGF, but not directly applicable to the nonsymmetrical components because of lack of closed-form expression for the subtracted part. However, for the nonsymmetrical components, the following equation can be used [24], [37]:

$$\int_0^\infty e^{-k_\rho\alpha} J_1(k_\rho\rho)dk_\rho = \frac{1}{\rho}\left(1-\frac{\alpha}{\sqrt{\alpha^2+\rho^2}}\right). \tag{9}$$

Equation (5) can then be written as

$$\begin{aligned} I_2 &= \int_0^\infty \left[\xi_2(k_\rho,k_{z,m})e^{-jk_{z,n}\alpha} - \tilde{\xi}_2 e^{-k_\rho\alpha} + \tilde{\xi}_2 e^{-k_\rho\alpha}\right] \\ &\qquad \times J_1(k_\rho\rho)dk_\rho \\ &= \int_0^\infty \left[\xi_2(k_\rho,k_{z,m})e^{-jk_{z,n}\alpha} - \tilde{\xi}_2 e^{-k_\rho\alpha}\right] J_1(k_\rho\rho)dk_\rho \\ &\qquad + \frac{\tilde{\xi}_2}{\rho}\left(1-\frac{\alpha}{\sqrt{\alpha^2+\rho^2}}\right) \end{aligned} \tag{10}$$

where $\tilde{\xi}_2 = \lim_{k_\rho\to\infty}\xi_2(k_\rho)$.

As a result, for the case where the source and field points are in the same layer (i.e., $m=n$), the subtraction procedure for the DGF can be formulated as follows:

$$\begin{aligned} G_{xx}^A &= \frac{1}{2\pi}\int_0^\infty \left[\tilde{G}_{xx}^A - \tilde{G}_{xx,\text{subt}}^A\right] J_0(k_\rho\rho)k_\rho dk_\rho + G_{xx,\text{add}}^A \\ G_{zz}^A &= \frac{1}{2\pi}\int_0^\infty \left[\tilde{G}_{zz}^A - \tilde{G}_{zz,\text{subt}}^A\right] J_0(k_\rho\rho)k_\rho dk_\rho + G_{zz,\text{add}}^A \\ G_{zx}^A &= \frac{1}{2\pi}\int_0^\infty \left[\tilde{G}_{zx}^A - \tilde{G}_{zx,\text{subt}}^A\right] J_1(k_\rho\rho)dk_\rho + G_{zx,\text{add}}^A \end{aligned} \tag{11}$$

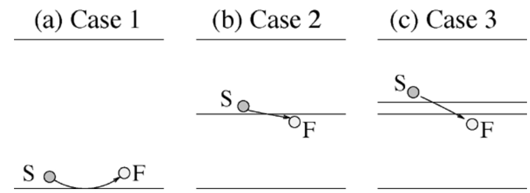

Fig. 2. (a) Case 1: source and field points are in the same layer. (b) Case 2: source and field points are in adjacent layers. (c) Case 3: there is one or more layers between source and field points.

where the subtracted integrands are

$$\begin{aligned} \tilde{G}_{xx,\text{subt}}^A &= \frac{1}{2jk_{z,n}}\tilde{A}_{0,1,2,3,4}^{\text{TE},1} \\ \tilde{G}_{zz,\text{subt}}^A &= \frac{1}{2jk_{z,n}}\left(\tilde{A}_{0,3,4}^{\text{TM},1} - \tilde{A}_{1,2}^{\text{TM},1}\right) \\ \tilde{G}_{zx,\text{subt}}^A &= \frac{1}{2j}\left(\tilde{A}_{1,4}^{\text{TE},2} - \tilde{A}_{2,3}^{\text{TE},2} - \tilde{A}_{1,4}^{\text{TM},2} + \tilde{A}_{2,3}^{\text{TM},2}\right) \end{aligned} \tag{12}$$

while the closed-form expressions for the subtracted terms are

$$\begin{aligned} G_{xx,\text{add}}^A &= \bar{A}_{0,1,2,3,4}^{\text{TE},1} \\ G_{zz,\text{add}}^A &= \bar{A}_{0,3,4}^{\text{TM},1} - \bar{A}_{1,2}^{\text{TM},1} \\ G_{zx,\text{add}}^A &= \bar{A}_{1,4}^{\text{TE},2} - \bar{A}_{2,3}^{\text{TE},2} - \bar{A}_{1,4}^{\text{TM},2} + \bar{A}_{2,3}^{\text{TM},2}. \end{aligned} \tag{13}$$

In the above,

$$\begin{aligned} \tilde{A}_i^{p,1} &= \tilde{a}_i^p e^{-jk_{z,n}\alpha_i} \\ \tilde{A}_i^{p,2} &= \tilde{a}_i^p e^{-k_\rho\alpha_i} \end{aligned} \tag{14}$$

$$\begin{aligned} \bar{A}_i^{p,1} &= \tilde{a}_i^p \frac{e^{-jk_{z,n}r_i}}{4\pi r_i} \\ \bar{A}_i^{p,2} &= \frac{\tilde{a}_i^p}{4\pi\rho}\left(1-\frac{\alpha_i}{r_i}\right) \end{aligned} \tag{15}$$

where $A_{i,\ldots,k} = A_i + \cdots + A_k$ and

$$\begin{aligned} \tilde{a}_0^p &= 1 \\ \tilde{a}_1^p &= R_{n,n+1}^p \\ \tilde{a}_2^p &= R_{n,n-1}^p, \\ \tilde{a}_3^p &= \tilde{a}_4^p = \tilde{a}_1^p\tilde{a}_2^p \end{aligned} \tag{16}$$

$$r_i = \sqrt{\rho^2+\alpha_i^2}. \tag{17}$$

The above subtraction procedure is very crucial when α_i is small, as the exponential term $e^{-jk_{z,n}\alpha_i}$ approaches one and does not decay with k_ρ when $\alpha_i \to 0$. In other words, when the source and field points are close to each other and close to an interface between two adjacent layers, the integrand decays slowly without subtraction. This situation is shown in Fig. 2 as case 1.

To demonstrate the importance of this subtraction, a six-layer geometry used in [6] is chosen as an example (Fig. 3). The integrand is calculated for some k_ρ values along the integration path illustrated in Fig. 4 [11]. The frequency is 30 GHz, $\rho = \lambda_0$ and $z = z' = 0.3 + \delta z$ mm, where $\delta z = \lambda_0/1000$. Fig. 5 depicts the magnitude of the integrand of the corresponding integral, i.e., $|\tilde{G}_{zx}^A J_1(k_\rho\rho)|$, the zx component of the DGF for vector potential $\mathbf{A}$, and the spectrum of $\tilde{G}_{zx}^A$ with and without subtraction. As can be seen from this figure, after subtraction, the integrand becomes a rapidly decreasing function of k_ρ. In fact, the decaying is exponential, and is six orders of magnitude smaller than the original integrand at $k_\rho = 10^6$.

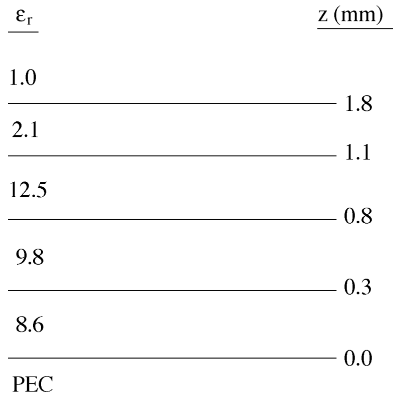

Fig. 3. Six-layer medium.

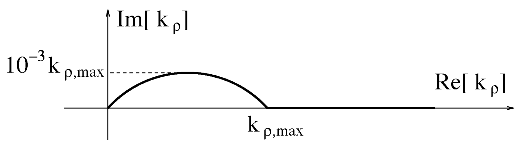

Fig. 4. Integration path in the complex k_ρ plane, $k_{\rho,\max} = 1.2\max\{k_1, k_2, \cdots, k_N\}$.

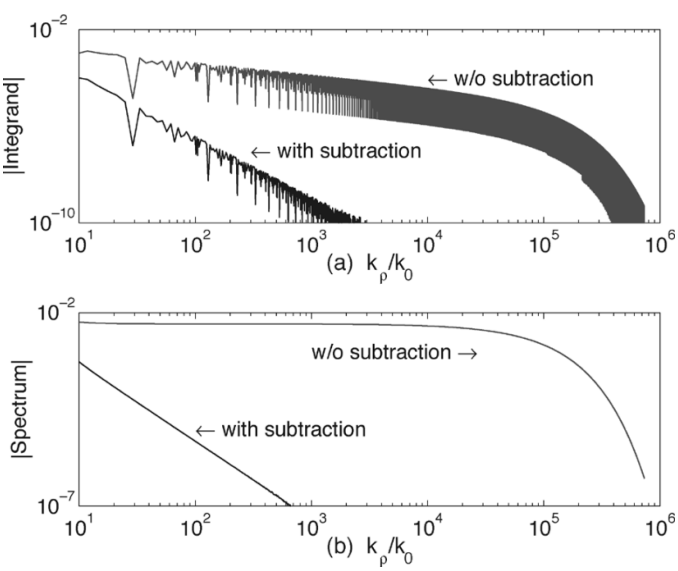

Fig. 5. (a) Magnitude of the integrand $\tilde{G}^A_{zx} J_1(k_\rho \rho)$ sampled along the integration path for $z = z' = 0.3 + \lambda_0/1000$ mm ($m = n$ case) for the six-layer medium depicted in Fig. 4. (b) The magnitude of the spectrum of $\tilde{G}^A_{zx}$.

The efficiency of this subtraction procedure becomes even more obvious as the source and field points get closer to the interface. Fig. 6 shows the number of segments used in the adaptive integration with and without subtraction for the same geometry with different δz values. Clearly, after the subtraction, the integrand decays rapidly no matter how small δz is, and the Green's functions are computed accurately by using only a few hundred integration segments or less.

To summarize the procedure for the $m = n$ case, the primary field term's contributions are calculated via the closed-form expressions for a homogeneous medium (also obtainable by using Sommerfeld identity) and, for each reflection term, the above subtraction procedure must be performed individually. Once the subtraction has been done, the integration of the remaining integrand can be calculated adaptively. In other words, the integral can be calculated segment by segment on the Sommerfeld integration path (SIP) until the desired accuracy is obtained.

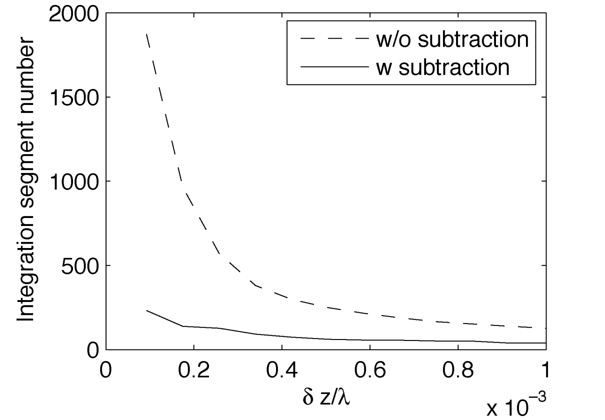

Fig. 6. Effect of subtraction on the convergence: the number of the segments used in adaptive integration with and without subtraction, $m = n$ case.

B. Source and Field Points in Different Layers

The above subtraction procedure is very efficient, but is restricted to the $m = n$ case. When source and field points are close to each other, but belonging to two different adjacent layers, shown in Case 2 in Fig. 2, some of the exponential terms' magnitudes are close to one, making the integrand an extremely slowly decaying function of k_ρ. Due to the different $k_{z,i}$ dependence, the Sommerfeld identity does not apply here. However, singularity subtraction is still possible by using the only common parameter: k_ρ. It is known that [29], [37]

$$\int_0^\infty e^{-k_\rho \alpha} J_0(k_\rho \rho) dk_\rho = \frac{1}{\sqrt{\alpha^2 + \rho^2}}. \tag{18}$$

Similar to the subtraction procedure described for nonsymmetrical components, using (7) and (18) in (4) yields

$$\begin{aligned} I_1 &= \int_0^\infty \left[\xi_1(k_\rho, k_{z,m}) e^{-jk_{z,n}\alpha} \frac{k_\rho}{k_{z,n}} - j\tilde{\xi}_1 e^{-k_\rho \alpha} + j\tilde{\xi}_1 e^{-k_\rho \alpha} \right] \\ &\quad \times J_0(k_\rho \rho) dk_\rho \\ &= \int_0^\infty \left[\xi_1(k_\rho, k_{z,m}) e^{-jk_{z,n}\alpha} \frac{k_\rho}{k_{z,n}} - j\tilde{\xi}_1 e^{-k_\rho \alpha} \right] J_0(k_\rho \rho) dk_\rho \\ &\quad + \frac{j\tilde{\xi}_1}{\sqrt{\alpha^2 + \rho^2}}. \end{aligned} \tag{19}$$

Since (9) and (18) have k_ρ dependence only, (10) and (19) are valid for any source–field layer combination. Note that for the $m = n$ case, there are five terms associated with TLGF and this number becomes ten when $m = n \pm 1$. The subtraction procedure must be performed appropriately for all those ten terms. For the $m = n - 1$ case, the subtracted integrands in (11) can be written as

$$\begin{aligned} \tilde{G}^A_{xx,\mathrm{subt}} &= \sum_{v=1}^{2} \frac{1}{2k_\rho} \tilde{B}^{\mathrm{TE},1}_{v0,1,2,3,4} \\ \tilde{G}^A_{zz,\mathrm{subt}} &= \sum_{v=1}^{2} \frac{1}{2k_\rho} \tilde{B}^{\mathrm{TM},1}_{v0,3,4} - \tilde{B}^{\mathrm{TM},1}_{v1,2} \\ \tilde{G}^A_{zx,\mathrm{subt}} &= \sum_{v=1}^{2} \frac{1}{2j} \left(\tilde{B}^{\mathrm{TE},2}_{v1,4} - \tilde{B}^{\mathrm{TE},2}_{v0,2,3} - \tilde{B}^{\mathrm{TM},2}_{v1,4} + \tilde{B}^{\mathrm{TM},2}_{v0,2,3} \right). \end{aligned} \tag{20}$$

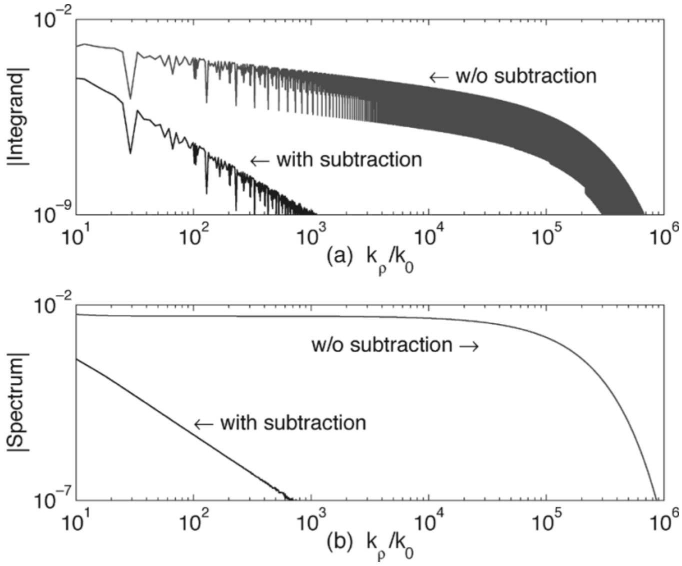

Fig. 7. (a) Magnitude of the integrand $\tilde{G}^A_{\mathbf{zx}} J_1(k_\rho \rho)$ sampled along the integration path for $z = (0.3 - \lambda_0/1000)$ mm, $z' = (0.3 + \lambda_0/1000)$ ($m = n - 1$ case) for the six-layer medium depicted in Fig. 4. (b) The magnitude of the spectrum of $\tilde{G}^A_{\mathbf{zx}}$.

The closed-form expressions for the subtracted integrals are

$$\begin{aligned} G^A_{xx,\mathrm{add}} &= \frac{\mu_n}{\mu_m} \sum_{v=1}^{2} \bar{B}^{\mathrm{TE},1}_{v0,1,2,3,4} \\ G^A_{zz,\mathrm{add}} &= \frac{\epsilon_m}{\epsilon_n} \sum_{v=1}^{2} \bar{B}^{\mathrm{TM},1}_{v0,3,4} - \bar{B}^{\mathrm{TM},1}_{v1,2} \\ G^A_{zx,\mathrm{add}} &= \sum_{v=1}^{2} \bar{B}^{\mathrm{TE},2}_{v1,4} - \bar{B}^{\mathrm{TE},2}_{v0,2,3} - \bar{B}^{\mathrm{TM},2}_{v1,4} + \bar{B}^{\mathrm{TM},2}_{v0,2,3}. \end{aligned} \tag{21}$$

In the above,

$$\begin{aligned} \tilde{B}^{p,1}_{1i} &= \tilde{a}^p_i e^{-k_\rho(\beta_1+\alpha_i)} \\ \tilde{B}^{p,2}_{1i} &= \tilde{a}^p_i e^{-k_\rho(\beta_1+\alpha_i)} \\ \tilde{B}^{p,1}_{2i} &= R_{m,m-1} \tilde{a}^p_i e^{-k_\rho(\beta_2+\alpha_i)} \\ \tilde{B}^{p,2}_{2i} &= R_{m,m-1} \tilde{a}^p_i e^{-k_\rho(\beta_2+\alpha_i)} \end{aligned} \tag{22}$$

$$\begin{aligned} \bar{B}^{p,1}_{1i} &= \frac{\tilde{a}^p_i}{4\pi r_{1i}} \\ \bar{B}^{p,2}_{1i} &= \frac{\tilde{a}^p_i}{4\pi\rho}\left(1 - \frac{\alpha_i + \beta_1}{r_{1i}}\right) \\ \bar{B}^{p,1}_{2i} &= R_{m,m-1} \frac{\tilde{a}^p_i}{4\pi r_{2i}} \\ \bar{B}^{p,2}_{2i} &= R_{m,m-1} \frac{\tilde{a}^p_i}{4\pi\rho}\left(1 - \frac{\alpha_i + \beta_2}{r_{2i}}\right) \end{aligned} \tag{23}$$

where $r_{vi} = \sqrt{\rho^2 + (\beta_v + \alpha_i)^2}$ and $v = 1, 2$

$$\beta_1 = z_m - z \quad \beta_2 = z_m + z - 2z_{m-1} \tag{24}$$

and $R_{m,m-1}$ is the Fresnel reflection coefficient and is independent of k_ρ.

This described procedure is as successful as the $m = n$ case. Fig. 7 depicts the magnitude of the integrand $|\tilde{G}^A_{zx} J_1(k_\rho \rho)|$ and the spectrum of $\tilde{G}^A_{zx}$ with and without subtraction when $z = (0.3 - \delta z)$ mm and $z' = (0.3 + \delta z)$ mm where $z = 0.3$ mm is the layer interface and $\delta z = \lambda_0/1000$. Again, after subtraction, the integrand becomes a rapidly decreasing function of k_ρ.

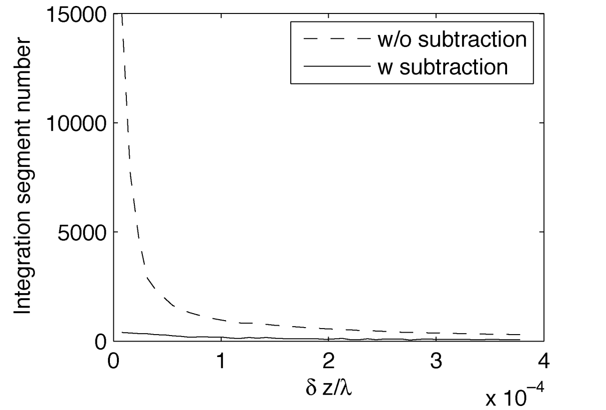

Fig. 8. Effect of subtraction on the convergence: the number of segments used in adaptive integration with and without subtraction, $m = n - 1$ case.

Similar to the experiment done for the $m = n$ case (Fig. 6), the efficiency of this subtraction procedure becomes even more significant as the source and field points get closer to the interface. Fig. 8 shows the number of the segments used in the adaptive integration with and without subtraction for the same geometry with different δz values for $\rho = \lambda_0$, $z' = 0.3 + \delta z$ mm and $z = 0.3 - \delta z$ mm where $z = 0.3$ mm is an interface of two adjacent layers shown in Fig. 4. Again, after the subtraction, the integrand decays rapidly (in fact, exponential) no matter how small δz is.

In the above, the formulation is presented for the $m = n$ and $m = n - 1$ cases. The formulation for the $m = n + 1$ case is very similar to the $m = n - 1$ case. This procedure can be extended to the $|m - n| > 1$ case easily by using asymptotic relations given by (7) with the help of the semi-infinite integral (9) and (18). For example, for the $m > n$ case, the terms to be subtracted can be formulated as

$$\begin{aligned} \tilde{G}^{p,VI}_{mn,\mathrm{subt}}(z|z') &= \tilde{T}^p_{V,mm} \tilde{T}^p_{V,mn} \tilde{G}^{p,VI}_{nn,\mathrm{subt}}(z_n|z') \\ \tilde{G}^{p,II}_{mn,\mathrm{subt}}(z|z') &= \tilde{T}^p_{I,mm} \tilde{T}^p_{V,mn} \tilde{G}^{p,VI}_{nn,\mathrm{subt}}(z_n|z') \\ \tilde{G}^{p,VV}_{mn,\mathrm{subt}}(z|z') &= \tilde{T}^p_{V,mm} \tilde{T}^p_{V,mn} \tilde{G}^{p,VV}_{nn,\mathrm{subt}}(z_n|z') \\ \tilde{G}^{p,IV}_{mn,\mathrm{subt}}(z|z') &= \tilde{T}^p_{I,mm} \tilde{T}^p_{V,mn} \tilde{G}^{p,VV}_{nn,\mathrm{subt}}(z_n|z') \end{aligned} \tag{25}$$

where

$$\tilde{G}^{p,VI}_{nn,\mathrm{subt}}(z|z') = \frac{\tilde{Z}^p_n}{2}\left\{\tilde{A}^{p,v}_0 + \tilde{A}^{p,v}_{1,2,3,4}\right\} \tag{26}$$

$$\tilde{G}^{p,II}_{nn,\mathrm{subt}}(z|z') = \frac{1}{2}\left\{\pm\tilde{A}^{p,v}_0 - \tilde{A}^{p,v}_{1,4} + \tilde{A}^{p,v}_{2,3}\right\} \tag{27}$$

$$\tilde{G}^{p,VV}_{nn,\mathrm{subt}}(z|z') = \frac{1}{2}\left\{\pm\tilde{A}^{p,v}_0 + \tilde{A}^{p,v}_{1,3} - \tilde{A}^{p,v}_{2,4}\right\} \tag{28}$$

$$\tilde{G}^{p,IV}_{nn,\mathrm{subt}}(z|z') = \frac{1}{2\tilde{Z}^p_n}\left\{\tilde{A}^{p,v}_0 - \tilde{A}^{p,v}_{1,2} + \tilde{A}^{p,v}_{3,4}\right\}. \tag{29}$$

$\tilde{A}^{p,v}_i$ is either $\tilde{A}^{p,1}_i$ or $\tilde{A}^{p,2}_i$ given by (14) depending on the order of the Bessel function and

$$\begin{aligned} \tilde{T}^p_{V,mm} &= \left(1 + R^p_{m,m+1} e^{-2k_\rho(z_m - z)}\right) e^{-k_\rho(z - z_{m-1})} \\ \tilde{T}^p_{I,mm} &= \tilde{Y}^p_m \left(1 - R^p_{m,m+1} e^{-2k_\rho(z_m - z)}\right) e^{-k_\rho(z - z_{m-1})} \end{aligned} \tag{30}$$

$$\tilde{T}^p_{V,mn} = \prod_{t=n+1}^{m-1} \left(1 + R^p_{t,t+1}\right) e^{-k_\rho d_t} \tag{31}$$

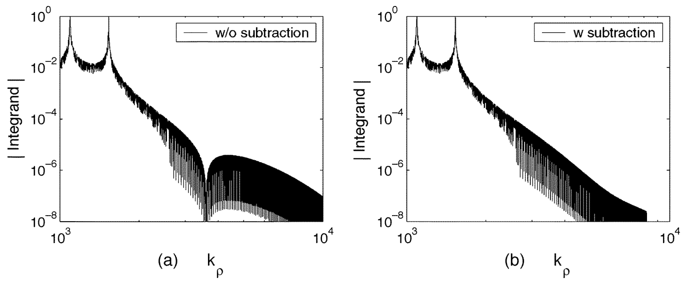

Fig. 9. Magnitude of the integrand $\tilde{G}_{zx}^{A} J_1(k_\rho \rho)$ sampled along the integration path for $z = 0.9$ mm, $z' = 0.2$ ($m = n + 2$ case) for the six-layer medium depicted in Fig. 4.

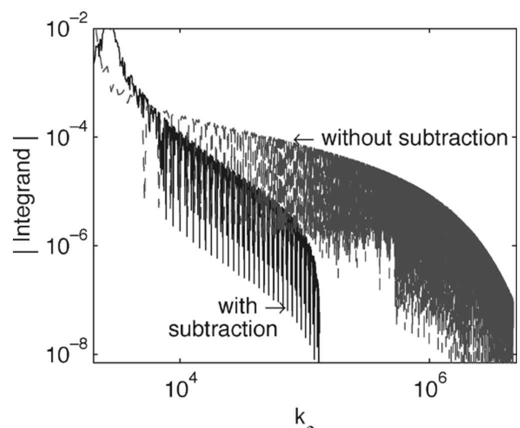

Fig. 10. Magnitude of the integrand $\tilde{G}_{zx}^{A} J_1(k_\rho \rho)$ sampled along the integration path for the seven-layer medium.

$$\begin{aligned} \tilde{Z}_i^{\mathrm{TE}} &= \frac{1}{\tilde{Y}_i^{\mathrm{TE}}} = \frac{\omega \mu_i}{k_\rho} \\ \tilde{Z}_i^{\mathrm{TM}} &= \frac{1}{\tilde{Y}_i^{\mathrm{TM}}} = \frac{k_\rho}{\omega \epsilon_i}. \end{aligned} \tag{32}$$

The number of the terms needs to be subtracted is ten for the $|m - n| > 1$ case. The effect of the subtraction may not be obvious for the problems having many thick layers and when the source and field points are very far away from each other. Under such circumstances, the integrand decays rapidly by itself and the subtraction procedure does not further improve the convergence; however, it does not degrade the convergence either since the subtracted terms also decay exponentially. For example, Fig. 9 shows the integrand $\tilde{G}_{zx}^{A} J_1(k_\rho \rho)$ with and without subtraction for $\rho = \lambda_0$, $z' = 0.2$ mm and $z = 0.9$ mm ($m = n + 2$) for the six-layer medium. Obviously, the subtraction procedure does not affect the decaying speed in a negative way. Usually, if d_t, the total thickness of the layers between the source and field points exceeds 10% of the local wavelength, such singularity subtraction does not have to be utilized. For a case where $|m - n| > 1$ and $d_t < 0.1\lambda_{\mathrm{local}}$, the extraction of the images becomes more effective as the $d_t/|z - z'|$ ratio gets closer to one and becomes less significant as the ratio gets closer to zero. Moreover, for problems with thin layers shown as Case 3 in Fig. 2, for very large values of ρ, the integral converges very slowly without singularity subtraction. As an example of the case $m = n + 2$, we study a seven-layer medium obtained by adding a very thin layer (thickness $= \lambda_0/10$, $\epsilon_r = 24$) between $z = 0.3$ mm and $z = 0.301$ mm on the six-layer medium in the previous example. Fig. 10 shows the integrand $\tilde{G}_{zx}^{A} J_1(k_\rho \rho)$ with and without subtraction when $\rho = 100\lambda_0$, $z' = (0.3 - \lambda_0/1000)$ mm and $z = (0.301 + \lambda_0/1000)$ mm for this seven-layer medium. Clearly, after subtraction, the integrand decays much more rapidly, indicating that the method is also useful for $|m - n| > 1$ if the ratio $d_t/|z - z'|$ is closer to one and the thickness between layers of z and z' is thin with respect to the wavelength.

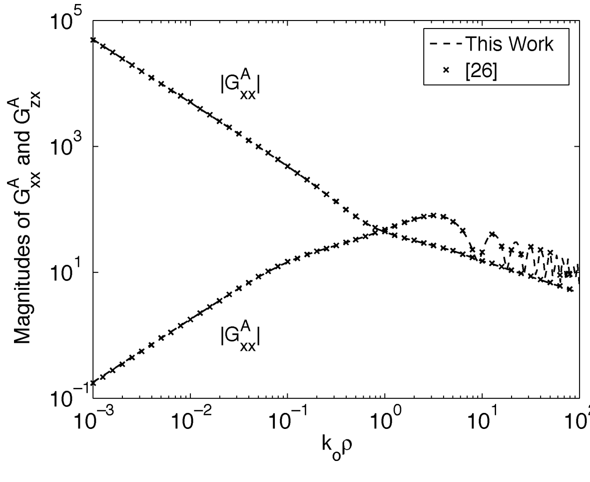

Fig. 11. Magnitudes of G_{xx}^{A} and G_{zx}^{A} compared with [26] for the six-layer medium with $z = z' = 0.4$ mm.

The above singularity subtraction is presented for $\mathbf{G}^{AJ}$. However, this method is valid for all types of Green's functions such as $\mathbf{G}^{EJ}$, $\mathbf{G}^{HJ}$, traditional or alternative form $\mathbf{G}^{A}$, and two- dimensional (2-D) Green's functions [36]. The asymptotic formulas required for these Green's functions are (9) and (18) and the following formulas and their derivatives:

$$\int_0^\infty e^{-k_\rho \gamma} k_\rho J_0(k_\rho \rho) dk_\rho = \frac{\gamma}{(\gamma^2 + \rho^2)^{\frac{3}{2}}} \tag{33}$$

$$\int_0^\infty e^{-k_\rho \gamma} k_\rho^2 J_0(k_\rho \rho) dk_\rho = \frac{2\gamma^2 - \rho^2}{(\gamma^2 + \rho^2)^{\frac{5}{2}}} \tag{34}$$

$$\int_0^\infty e^{-k_\rho \gamma} k_\rho J_1(k_\rho \rho) dk_\rho = \frac{\rho}{(\gamma^2 + \rho^2)^{\frac{3}{2}}} \tag{35}$$

$$\int_0^\infty e^{-k_\rho \gamma} k_\rho^2 J_1(k_\rho \rho) dk_\rho = \frac{3\gamma\rho}{(\gamma^2 + \rho^2)^{\frac{5}{2}}}. \tag{36}$$

IV. Numerical Results

The described technique has been implemented for several types of 2-D and three-dimensional (3-D) spatial-domain Green's functions. Since 2-D results have been presented in [36], only 3-D examples are presented here. The first two examples are chosen to demonstrate the accuracy of the method. The first example (Fig. 11) shows the magnitude of the traditional form of Green's functions associated with the magnetic vector potential. The geometry is the six-layer medium shown in Fig. 4. The frequency is 30 GHz and $z = z' = 0.4$ mm. Fig. 12 is obtained by using the same geometry parameters, except that $z = 1.4$ mm.

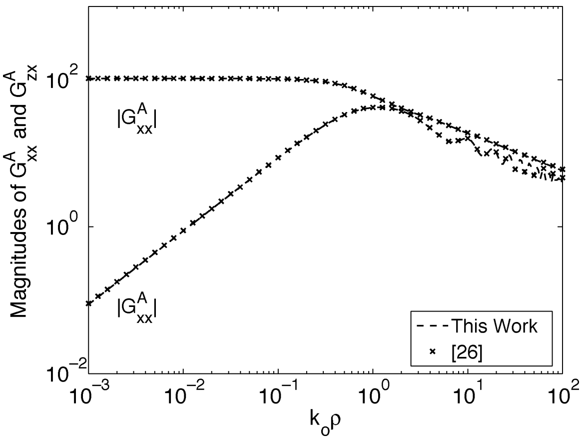

Fig. 12. Magnitudes of G^A_{xx} and G^A_{zx} compared with [26] for the six-layer medium with $z' = 0.4$ mm, $z = 1.4$ mm.

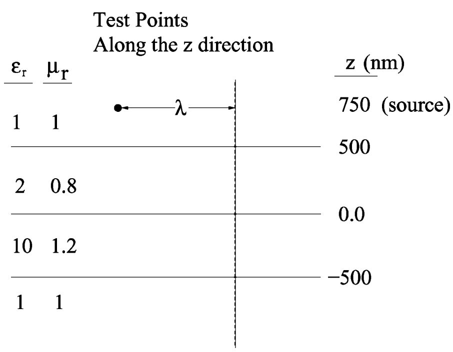

Fig. 13. Four-layer medium.

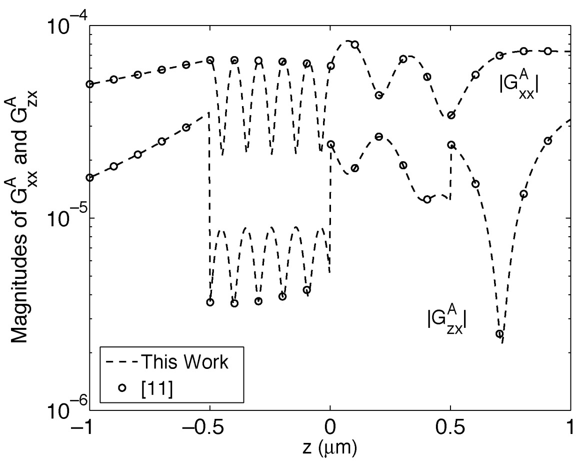

Fig. 14. Magnitudes of G^{EJ}_{xx} and G^{EJ}_{zx} compared with [11] for the four-layer medium with $z' = 750$ nm, $z = [-1000, 1000]$ nm.

For the four-layer medium shown in Fig. 13, Fig. 14 shows the magnitude of the different type of Green's functions $(\mathbf{G}^{EJ})$. The wavelength in the free space is 633 nm and the source is located at $z' = 750$ nm. The field points are chosen from $z = -1000$ nm to $z = 1000$ nm.

In all these figures, the results are calculated using the described procedure and compared with those obtained by direct numerical integration along the SIP. In all cases, excellent agreement has been verified.

Another issue is the efficiency. To demonstrate the efficiency of the method, a five-layer geometry is chosen as Fig. 15. The

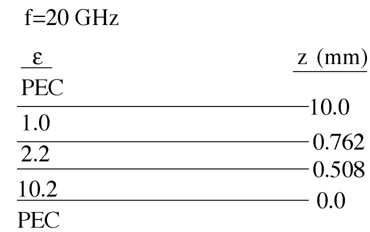

Fig. 15. Five-layer medium.

TABLE I
EXPERIMENT RESULTS

z' (mm)	z (mm)	ρ/λ_0	CPU (s) W/O	CPU (s) W/
0.7622	0.7618	0.1	1.63	0.31
0.7622	0.7618	1	147	0.98
0.508	0.507	1	49	0.47
0.508	0.507	10	131	0.98

Green's function $\mathbf{G^A}$ is calculated with and without subtraction for different z, z', and ρ values. Both programs were compiled with a Fortran77 UNIX compiler on a Dell Optiplex GX260 desktop with an Intel P4 2.4-GHz processor and 1024-MB RAM. The last two columns of Table I show the CPU times with and without subtraction for the same accuracy level (10^{-9}). With the classical numerical integration, depending on z, z', and ρ, the execution time changes dramatically. For large ρ values, it may take more than 2 min just for one sample, whereas it takes less than 1 s with this described method even for $\rho = 10\lambda$.

The efficient computation of the DGFs for layered media is an important part of fast forward and inverse scattering problems for 3-D targets buried in such environments (see, e.g., [38] and [39]).

V. Conclusion

In this paper, a numerically efficient way of evaluating the multilayer medium Green's functions has been presented. The singularity terms that cause slow convergence have been subtracted analytically. No matter how close the source and field points are to an interface or no matter how large ρ is, the described subtraction procedure makes the integrand a rapidly decreasing function of k_ρ. Since the remaining integral is calculated numerically as accurately as desired, the complete procedure is error controllable and a robust method. The accuracy and efficiency of the method have been verified via representative numerical examples.

Appendix

The spectral-domain Green's functions for vector potential $\mathbf{A}$ can be formulated as follows [33]:

$$\widetilde{\mathbf{G}}^{\mathbf{A}} = \begin{bmatrix} \tilde{G}^A_{xx} & 0 & 0 \\ 0 & \tilde{G}^A_{xx} & 0 \\ \tilde{G}^A_{zx} & \tilde{G}^A_{zy} & \tilde{G}^A_{zz} \end{bmatrix} \tag{37}$$

$$\tilde{G}^A_{xx} = \frac{1}{j\omega\mu_m}\tilde{G}^{\mathrm{TE},VI}_{mn} \tag{38}$$

$$\tilde{G}^A_{zz} = \frac{1}{j\omega\epsilon_n}\tilde{G}^{\mathrm{TM},IV}_{mn} \tag{39}$$

$$\tilde{G}^{A}_{zx} = \frac{k_x}{jk_\rho^2}\left(\tilde{G}^{\mathrm{TE},II}_{mn} - \tilde{G}^{\mathrm{TM},II}_{mn}\right) \tag{40}$$

where $\tilde{G}^{p,QR}_{mn}$ is the p-type (TE or TM) TLGF relating Q (voltage or current) at z in layer m due to an R-type (voltage or current) unit source at z' in layer n. The formulas of the TLGFs depending on location of the source and field points can be given as follows.

A. $m = n$

When source and field points belong to the same layer,

$$\tilde{G}^{p,VI}_{nn}(z|z') = \frac{Z^p_n}{2}\left\{A^p_0 + \frac{A^p_{1,2,3,4}}{D^p_n}\right\} \tag{41}$$

$$\tilde{G}^{p,II}_{nn}(z|z') = \frac{1}{2}\left\{\pm A^p_0 + \frac{\left(A^p_{2,3} - A^p_{1,4}\right)}{D^p_n}\right\} \tag{42}$$

$$\tilde{G}^{p,VV}_{nn}(z|z') = \frac{1}{2}\left\{\pm A^p_0 + \frac{\left(A^p_{1,3} - A^p_{2,4}\right)}{D^p_n}\right\} \tag{43}$$

$$\tilde{G}^{p,IV}_{nn}(z|z') = \frac{1}{2Z^p_n}\left\{A^p_0 + \frac{\left(A^p_{3,4} - A^p_{1,2}\right)}{D^p_n}\right\} \tag{44}$$

where p is either TE or TM, and the sign of the primary field term is positive when $z > z'$, otherwise it is negative. In the above, $A_{i,\cdots,k} = A_i + \cdots + A_k$

$$A^p_i = a^p_i e^{-jkz_{z,n}\alpha_i}, \qquad i = 0,1,2,3,4 \tag{45}$$

$$\begin{aligned} Z^{\mathrm{TE}}_i &= \frac{1}{Y^{\mathrm{TE}}_i} = \frac{\omega\mu_i}{k_{z,i}} \\ Z^{\mathrm{TM}}_i &= \frac{1}{Y^{\mathrm{TM}}_i} = \frac{k_{z,i}}{\omega\epsilon_i} \end{aligned} \tag{46}$$

$$\begin{aligned} r_i &= \sqrt{\rho^2 + \alpha_i^2} \\ \alpha_0 &= |z - z'| \\ a^p_0 &= 1 \\ \alpha_1 &= 2z_n - (z + z') \\ a^p_1 &= \Gamma^p_{n,n+1} \\ \alpha_2 &= (z + z') - 2z_{n-1} \\ a^p_2 &= \Gamma^p_{n,n-1} \\ \alpha_3 &= 2d_n - \alpha_0 \\ a^p_3 &= a^p_1 a^p_2 \\ \alpha_4 &= 2d_n + \alpha_0 \\ a^p_4 &= a^p_3 \\ D^p_n &= 1 - a^p_3 e^{-j2k_{z,n}d_n} \end{aligned} \tag{47}$$

where $\Gamma^p_{i,j}$ is the p-type generalized reflection coefficients which can be calculated recursively by using [35]

$$\Gamma^p_{i,i+1} = \frac{R^p_{i,i+1} + \Gamma^p_{i+1,i+2}e^{-j2k_{z,i+1}d_{i+1}}}{1 + R^p_{i,i+1}\Gamma^p_{i+1,i+2}e^{-j2k_{z,i+1}d_{i+1}}} \tag{48}$$

d_i is the width of the ith layer. $R^p_{i,i+1}$ denotes the p-type Fresnel reflection coefficient given by

$$R^{\mathrm{TM}}_{i,i+1} = \frac{\epsilon_{r,i+1}k_{z,i} - \epsilon_{r,i}k_{z,i+1}}{\epsilon_{r,i+1}k_{z,i} + \epsilon_{r,i}k_{z,i+1}} \tag{49}$$

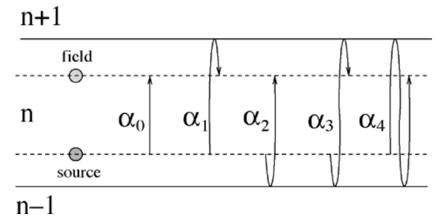

Fig. 16. Physical demonstration of primary and quasi-static field terms.

$$R^{\mathrm{TE}}_{i,i+1} = \frac{\mu_{r,i+1}k_{z,i} - \mu_{r,i}k_{z,i+1}}{\mu_{r,i+1}k_{z,i} + \mu_{r,i}k_{z,i+1}}. \tag{50}$$

Fig. 16 shows where these primary field and reflection terms come from.

B. $m > n$

When source and field points are in different layers, the spectral-domain Green's function can be computed by using voltage/current transfer functions as follows:

$$\begin{aligned} \tilde{G}^{p,VI}_{mn}(z|z') &= T^p_{V,mm}T^p_{V,mn}\tilde{G}^{p,VI}_{nn}(z_n|z') \\ \tilde{G}^{p,II}_{mn}(z|z') &= T^p_{I,mm}T^p_{V,mn}\tilde{G}^{p,VI}_{nn}(z_n|z') \\ \tilde{G}^{p,VV}_{mn}(z|z') &= T^p_{V,mm}T^p_{V,mn}\tilde{G}^{p,VV}_{nn}(z_n|z') \\ \tilde{G}^{p,IV}_{mn}(z|z') &= T^p_{I,mm}T^p_{V,mn}\tilde{G}^{p,VV}_{nn}(z_n|z') \end{aligned} \tag{51}$$

where $T_{P,mm}$ denotes the P-type (either voltage or current) transfer function between a point z in layer m and the lower boundary of that layer z_{m-1}, and $T_{V,mn}$ denotes the voltage transfer function between z_{m-1} and the upper boundary of the nth layer z_n. Multiplication of these two terms with $\tilde{G}^p_{nn}(z_n|z')$ gives $\tilde{G}^p_{nn}(z|z')$

$$\begin{aligned} T^p_{V,mm} &= \frac{\left[1 + \Gamma^p_{m,m+1}e^{-j2k_{zm}(z_m - z)}\right]e^{-jk_{zm}(z - z_{m-1})}}{1 + \Gamma^p_{m,m+1}e^{-j2k_{zm}d_m}} \\ T^p_{I,mm} &= Y^p_m\frac{\left[1 - \Gamma^p_{m,m+1}e^{-j2k_{zm}(z_m - z)}\right]e^{-jk_{zm}(z - z_{m-1})}}{1 + \Gamma^p_{m,m+1}e^{-j2k_{zm}d_m}} \end{aligned} \tag{52}$$

$$T^p_{V,mn} = \prod_{t=n+1}^{m-1}\frac{\left(1 + \Gamma^p_{t,t+1}\right)e^{-jk_{zt}d_t}}{1 + \Gamma^p_{t,t+1}e^{-j2k_{zt}d_t}}. \tag{53}$$

Note that $T^p_{V,mn} = 1$ when $m = n + 1$.

C. $m < n$

Similarly, for $m < n$ case,

$$\begin{aligned} &\tilde{G}^{p,VI}_{mn}(z|z') \\ &\quad = T^p_{V,mm}T^p_{V,mn}\tilde{G}^{p,VI}_{nn}(z_{n-1}|z') \\ &\tilde{G}^{p,II}_{mn}(z|z') \\ &\quad = T^p_{I,mm}T^p_{V,mn}\tilde{G}^{p,VI}_{nn}(z_{n-1}|z') \\ &\tilde{G}^{p,VV}_{mn}(z|z') \\ &\quad = T^p_{V,mm}T^p_{V,mn}\tilde{G}^{p,VV}_{nn}(z_{n-1}|z') \\ &\tilde{G}^{p,IV}_{mn}(z|z') \\ &\quad = T^p_{I,mm}T^p_{V,mn}\tilde{G}^{p,VV}_{nn}(z_{n-1}|z') \end{aligned} \tag{54}$$

$$T^p_{V,mm} = \frac{\left[1+\Gamma^p_{m,m-1}e^{-j2k_{zm}(z-z_{m-1})}\right]e^{-jk_{zm}(z_m-z)}}{1+\Gamma^p_{m,m-1}e^{-j2k_{zm}d_m}}$$

$$T^p_{I,mm} = -Y^p_m \frac{\left[1-\Gamma^p_{m,m-1}e^{-j2k_{zm}(z-z_{m-1})}\right]e^{-jk_{zm}(z_m-z)}}{1+\Gamma^p_{m,m-1}e^{-j2k_{zm}d_m}} \tag{55}$$

$$T^p_{V,mn} = \prod_{t=m+1}^{n-1} \frac{\left(1+\Gamma^p_{t,t-1}\right)e^{-jk_{zt}d_t}}{1+\Gamma^p_{t,t-1}e^{-j2k_{zt}d_t}}. \tag{56}$$

Note that $T^p_{V,mn}=1$ when $m=n+1$.

REFERENCES

[1] K. A. Michalski and D. Zheng, "Electromagnetic scattering and radiation by surfaces of arbitrary shape in layered media: Part II: Implementation and results for contiguous half-spaces," *IEEE Trans. Antennas Propag.*, vol. 38, no. 3, pp. 345–352, Mar. 1990.

[2] T. J. Cui and W. C. Chew, "Fast evaluation of Sommerfeld integrals for EM scattering and radiation by three-dimensional buried objects," *IEEE Trans. Geosci. Remote Sens.*, vol. 37, no. 3, pp. 887–900, Mar. 1999.

[3] N. Geng and L. Carin, "Wide-band electromagnetic scattering from a dielectric BOR buried in a layered lossy dispersive medium," *IEEE Trans. Antennas Propag.*, vol. 47, no. 4, pp. 610–619, Apr. 1999.

[4] J. R. Mosig, "Arbitrarily shaped microstrip structures and their analysis with a mixed potential integral equation," *IEEE Trans. Microw. Theory Tech.*, vol. 36, no. 2, pp. 314–323, Feb. 1988.

[5] D. Zheng and K. A. Michalski, "Analysis of coaxially fed microstrip antennas of arbitrary shape with thick substrates," *J. Electromagn. Waves Applicat.*, vol. 5, no. 12, pp. 1303–1327, 1991.

[6] J. M. Jin, J. Liu, and F. Ling, "Efficient electromagnetic modeling of 3-D multilayer microstrip antennas and circuits," *IEEE Trans. Microw. Theory Tech.*, vol. 50, no. 6, pp. 1628–1635, Jun. 2002.

[7] A. Sommerfeld, *Partial Differential Equations in Physics*. New York: Academic, 1949.

[8] J. R. Mosig and F. E. Gardiol, "Analytic and numerical techniques in the Green's function treatment of microstrip antennas and scatterers," *Proc. Inst. Elect. Eng.*, pt. H, vol. 130, pp. 175–182, Mar. 1983.

[9] ——, "General integral equation formulation for microstrip antennas and scatterers," *Proc. Inst. Elect. Eng.*, pt. H, vol. 132, pp. 424–432, Dec. 1985.

[10] N. K. Das and D. M. Pozar, "A generalized spectral-domain Green's function for the multilayer dielectric substrates with application to multilayer transmission lines," *IEEE Trans. Microw. Theory Tech.*, vol. MTT-35, no. 3, pp. 326–335, Mar. 1987.

[11] M. Paulus, P. Gay-Balmaz, and O. J. F. Martin, "Accurate and efficient computation of the Green's tensor for stratified media," *Phys. Rev.*, vol. 62, no. 4, pp. 5797–5807, Oct. 2000.

[12] J. Zhao, S. Kapur, D. E. Long, and W. W. M. Dai, "Efficient three-dimensional extraction based on static and full wave layered Green's functions," presented at the Proc. 35th Design Automation Conf., Jun. 1998.

[13] L. Tsang, C. Ong, C. C. Huang, and V. Jandhyala, "Evaluation of the Green's function for the mixed potential integral equation (MPIE) method in the time domain for layered media," *IEEE Trans. Antennas Propag.*, vol. 51, no. 7, pp. 1559–1571, Jul. 2003.

[14] W. Cai and T. Yu, "Fast calculations of dyadic Green's functions for electromagnetic scattering in a multilayer medium," *J. Comput. Phys.*, vol. 165, pp. 1–21, 2000.

[15] I. V. Lindell and E. Alanen, "Exact image theory for the Sommerfeld half space problem—Part 1: Vertical magnetic dipole," *IEEE Trans. Antennas Propag.*, vol. AP-32, no. 2, pp. 126–132, Feb. 1984.

[16] ——, "Exact image theory for the Sommerfeld half space problem—Part 2: Vertical electric dipole," *IEEE Trans. Antennas Propag.*, vol. AP-32, no. 10, pp. 841–849, Oct. 1984.

[17] D. G. Fang, J. J. Yang, and G. Y. Delisle, "Discrete image theory for horizontal electric dipoles in a multilayered medium," *Proc. Inst. Elect. Eng.*, pt. H, vol. 135, pp. 297–303, Oct. 1988.

[18] Y. L. Chow, J. J. Yang, D. G. Fang, and G. E. Howard, "A closed-form spatial Green's function for the thick substrate," *IEEE Trans. Microw. Theory Tech.*, vol. 39, no. 3, pp. 588–592, Mar. 1991.

[19] M. I. Aksun and R. Mittra, "Derivation of closed-form Green's functions for a general microstrip geometry," *IEEE Trans. Microw. Theory Tech.*, vol. 40, no. 11, pp. 2055–2062, Nov. 1992.

[20] R. A. Kipp, C. H. Chan, A. T. Yang, and J. T. Yao, "Simulation of high frequency integrated circuits incorporating full wave analysis of microstrip discontinuities," *IEEE Trans. Microw. Theory Tech.*, vol. 41, no. 5, pp. 848–854, May 1993.

[21] R. A. Kipp and C. H. Chan, "Complex image method for sources in bounded regions of multilayer structures," *IEEE Trans. Microw. Theory Tech.*, vol. 42, no. 5, pp. 860–865, May 1994.

[22] G. Dural and M. I. Aksun, "Closed-form Green's functions for general sources in stratified media," *IEEE Trans. Microw. Theory Tech.*, vol. 43, no. 7, pp. 1545–1552, Jul. 1995.

[23] M. I. Aksun, "A robust approach for the derivation of the closed-form Green's functions," *IEEE Trans. Microw. Theory Tech.*, vol. 44, no. 5, pp. 651–658, May 1996.

[24] N. Hojjat, S. Safavi-Naeini, and Y. L. Chow, "Numerical computation of complex image Green's functions for multilayer dielectric media: Near field zone and the interface region," *Proc. Inst. Elect. Eng.—Microwave Antennas Propag.*, vol. 145, no. 6, pp. 449–454, Dec. 1998.

[25] N. Hojjat, S. Safavi-Naeini, R. F. Dana, and Y. L. Chow, "Fast computation of the nonsymmetrical components of the Green's functions for multilayer dielectric media using complex images," *Proc. Inst. Elect. Eng.—Microwave Antennas Propag.*, vol. 145, no. 6, pp. 285–289, Aug. 1998.

[26] F. Ling, "Fast electromagnetic modeling of multilayer microstrip antennas and circuits," Ph.D. dissertation, Dept. Elect. Comput. Eng., Univ. Illinois at Urbana-Champaign, Urbana, IL, 2000.

[27] A. A. K. Mohsen and A. K. Abdelmageed, "An efficient evaluation of the nonsymmetrical components of the Green's function for multilayered media," *Microwave Opt. Technol. Lett.*, vol. 28, no. 3, pp. 199–202, 2001.

[28] Y. Liu, L. W. Li, T. Yeo, and M. S. Leong, "Application of DCIM to MPIE–MoM analysis of 3-D PEC objects in multilayered media," *IEEE Trans. Antennas Propag.*, vol. 50, no. 2, pp. 157–162, Feb. 2002.

[29] K. P. Eselle and Y. Ge, "New closed-form Green's functions for microstrip structures—Theory and results," *IEEE Trans. Microw. Theory Tech.*, vol. 50, no. 6, pp. 1556–1560, Jun. 2002.

[30] K. A. Michalski and D. Zheng, "Electromagnetic scattering and radiation by surfaces of arbitrary shape in layered media: Part I: Theory," *IEEE Trans. Antennas Propag.*, vol. 38, no. 3, pp. 335–344, Mar. 1990.

[31] ——, "Electromagnetic scattering and radiation by surfaces of arbitrary shape in layered media: Part II: Implementation and results for contiguous half-spaces," *IEEE Trans. Antennas Propag.*, vol. 38, no. 3, pp. 355–352, Mar. 1990.

[32] ——, "Analysis of microstrip resonators of arbitrary shape," *IEEE Trans. Microw. Theory Tech.*, vol. 10, no. 1, pp. 112–119, Jan. 1992.

[33] K. A. Michalski and J. R. Mosig, "Multilayered media Green's functions in integral equation formulations," *IEEE Trans. Antennas Propag.*, vol. 45, no. 3, pp. 508–519, Mar. 1997.

[34] P. Ylä-Oijala, M. Taskinen, and J. Sarvas, "Multilayered media Green's functions for MPIE with general electric and magnetic sources by the Hertz potential approach," *Progr. Electromagn. Res.*, vol. 33, pp. 141–165, 2001.

[35] W. C. Chew, *Waves and Fields in Inhomogeneous Media*. Piscataway, NJ: IEEE Press, 1995.

[36] E. Simsek and Q. H. Liu, "Fast computation of dyadic Green's function for layered media and its application in interconnect simulations," in *IEEE AP-S Symp.*, vol. 3, Jun. 2004, p. 2783.

[37] I. S. Gradshteyn and I. M. Ryzhik, *Table of Integrals, Series, and Products*. New York: Academic, 1965.

[38] X. Millard and Q. H. Liu, "A fast volume integral equation solver for electromagnetic scattering from large inhomogeneous objects in planarly layered media," *IEEE Trans. Antennas Propag.*, vol. 51, no. 9, pp. 2393–2401, Sep. 2003.

[39] F. Li, Q. H. Liu, and L.-P. Song, "Three-dimensional reconstruction of objects buried in layered media using Born and distorted Born iterative methods," *IEEE Geosci. Remote Sens. Lett.*, vol. 1, no. 2, pp. 107–111, Feb. 2004.

Ergün Şimşek (S'01) received the B.A. degree in electrical engineering from Bilkent University, Ankara, Turkey, in 2001, the M.S. degree in electrical and computer engineering from the University of Massachusetts Dartmouth, in 2003, and is currently working toward the Ph.D. degree at Duke University, Durham, NC.

Since 2003, he has been a Research Assistant with Duke University. His research interests include numerical methods and computational electromagnetics.

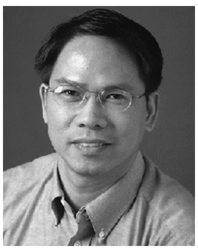

Qing Huo Liu (S'88–M'89–SM'94–F'05) received the Ph.D. degree in electrical engineering from the University of Illinois at Urbana-Champaign, in 1989.

From September 1986 to December 1988, he was a Research Assistant with the Electromagnetics Laboratory, University of Illinois at Urbana-Champaign, and from January 1989 to February 1990, he was a Post-Doctoral Research Associate. From 1990 to 1995, he was a Research Scientist and Program Leader with Schlumberger-Doll Research, Ridgefield, CT. From 1996 to May 1999, he was an Associate Professor with New Mexico State University. Since June 1999, he has been with Duke University, Durham, NC, where he is currently a Professor of electrical and computer engineering. He has authored or coauthored over 300 papers in refereed journals and conference proceedings. His research interests include computational electromagnetics and acoustics, inverse problems, geophysical subsurface sensing, biomedical imaging, electronic packaging, and the simulation of photonic devices and nanodevices. He is an Associate Editor for *Radio Science*.

Dr. Liu is a Fellow of the Acoustical Society of America. He is a member of Phi Kappa Phi, Tau Beta Pi. He is a full member of the U.S. National Committee of URSI Commissions B and F. He currently serves as an associate editor for the IEEE TRANSACTIONS ON GEOSCIENCE AND REMOTE SENSING, for which he also served as a guest editor for a Special Issue on Computational Methods. He was the recipient of the 1996 Presidential Early Career Award for Scientists and Engineers (PECASE) presented by the White House, the 1996 Early Career Research Award presented by the Environmental Protection Agency, and the 1997 CAREER Award presented by the National Science Foundation (NSF).

Baojun Wei received the B.A. degree in physics from Beijing Normal University, Beijing, China, in 1991, and the M.S. and Ph.D. degrees in geophysics from the University of Petroleum, Shandong, China, in 1997 and 2003, respectively.

From July 1991 to July 2004, he taught and performed research with the University of Petroleum. Since July 2004, he has been a Post-Doctoral Research Associate with the Department of Electrical and Computer Engineering, Duke University, Durham, NC. His research interests are forward modeling and inversion methods in electromagnetics.